First publ. in: Biochimica et Biophysica Acta / Molecular cell research, 1783 (2008), 6, pp. 1076–1084

The deletion of amino acids 114–121 in the TM1 domain of mouse prion protein stabilizes its conformation but does not affect the overall structure

Bastian Thaa [a], Ralph Zahn [b], Ulrich Matthey [b], Peter M.H. Kroneck [a], Alexander Bürkle [a,*], Günter Fritz [a,*]

[a] *Fachbereich Biologie, Mathematisch-Naturwissenschaftliche Sektion, Universität Konstanz, 78457 Konstanz, Germany*
[b] *Alicon AG, Wagistrasse 23, CH-8952 Schlieren, Switzerland*

Abstract

A mutant of mouse prion protein (PrP^C) carrying a deletion of residues 114–121 (PrPΔ114–121) has previously been described to lack convertibility into the scrapie-associated isoform of PrP (PrP^{Sc}) and to exhibit a dominant-negative effect on the conversion of wild-type PrP^C into PrP^{Sc} in living cells. Here we report the characterization of recombinantly expressed PrPΔ114–121 by Fourier-transformation infrared spectroscopy (FTIR) and circular dichroism (CD) spectroscopy. The analysis of spectra revealed an increased antiparallel β-sheet content in the deletion mutant compared to wild-type PrP^C. This additional short β-sheet stabilized the fold of the mutant protein by $\Delta\Delta G^{0\prime}=3.4\pm0.3$ kJ mol^{-1} as shown by chemical unfolding experiments using guanidine hydrochloride. Secondary structure predictions suggest that the additional β-sheet in PrPΔ114–121 is close to the antiparallel β-sheet in PrP^C. The high-affinity Cu^{2+}-binding site outside the octarepeats, which is located close to the deletion and involves His110 as a ligand, was not affected, as detected by electron paramagnetic resonance (EPR) spectroscopy, suggesting that Cu^{2+} binding does not contribute to the protection of PrPΔ114–121 from conversion into PrP^{Sc}. We propose that the deletion of residues 114–121 stabilizes the mutant protein. This stabilization most likely does not obstruct the interaction of PrPΔ114–121 with PrP^{Sc} but represents an energy barrier that blocks the conversion of PrPΔ114–121 into PrP^{Sc}.

Keywords: Prion; Deletion mutant; Fourier transformed infrared spectoscopy FTIR; Circular dichrosim CD; Copper; EPR

1. Introduction

Prions are the causative agents of transmissible spongiform encephalopathies [1]. These fatal neurodegenerative diseases include BSE in cattle, scrapie in sheep, and Creutzfeldt–Jakob disease (CJD) in humans, and can be of infectious or genetic etiology or arise spontaneously. They are characterized by the conversion of the cellular prion protein (PrP^C) into a disease-associated isoform (PrP^{Sc}), which shows an increased β-sheet content, resistance to proteinase K, insolubility in detergents and a tendency to aggregate. It is assumed that the conversion of PrP^C to PrP^{Sc} entails the formation of a PrP^C–PrP^{Sc} heterodimer [2], in which PrP^{Sc} catalyzes the conversion of PrP^C into PrP^{Sc}. Although PrP^{Sc} accumulation is a hallmark of prion diseases, it is probably not the neurotoxic molecule *per se* [3], since PrP^{Sc} proved non-toxic to neurons that are lacking PrP^C expression [4,5].

PrP^C, whose expression is essential for the susceptibility to prion infection [6], is mainly expressed in neurons and is a highly conserved cell surface protein, attached to the outer leaflet of the cell membrane via a C-terminal glycosyl-phosphatidylinositol (GPI) anchor. Its physiological function remains to be elucidated, but its ability to selectively bind Cu^{2+} has been documented in numerous studies [7,8]. Cu^{2+} binding is mediated by the N-terminal octarepeats (amino acid sequence PHGGGWGQ) and a region close to the transmembrane (TM1) domain involving His110 (mouse numbering) [9] (Fig. 1). In

* Corresponding authors. A. Bürkle is to be contacted at Fachbereich Biologie, Fach X911, Universität Konstanz, Germany. Tel.: +49 7531 88 4034; fax: +49 7531 88 4033. G. Fritz, Fachbereich Biologie, Fach M665, Universität Konstanz, Germany. Tel.: +49 7531 88 3205; fax: +49 7531 88 2966.
E-mail addresses: alexander.buerkle@uni-konstanz.de (A. Bürkle), guenter.fritz@uni-konstanz.de (G. Fritz).

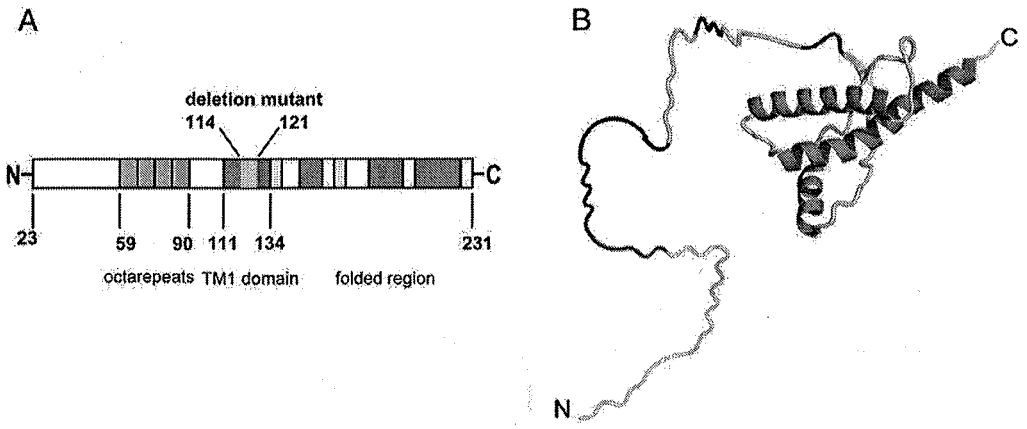

Fig. 1. Location of deletion mutation in PrP. (A) Schematic representation of PrP^C domain structure. The TM1 domain is shown in blue, deletion of aa 114–121 in cyan; location of α-helices are indicated in red and location of β-sheets in yellow. (B) Model of PrP^C using the same color code as in panel A. The N-terminal domain of PrP^C (aa 23–126), which has not been characterized structurally, is shown as an extended loop structure; the location of the octarepeats within this region is shown in dark grey; α-helices are shown in red and β-sheets in yellow.

addition to the membrane localization via the GPI anchor of PrP^C, transmembrane topologies of PrP^C have been described [10,11]. These transmembrane forms are inserted into the lipid bilayer of the endoplasmic reticulum via the TM1 domain of PrP^C, a hydrophobic stretch between residues 111 and 134, encompassing the highly conserved hydrophobic core AGAAAAGA (amino acids 112–119).

The first link between the TM1 domain and prion disease became apparent by the fact that a peptide encompassing amino acids 106–126 (human numbering) induces neurotoxic effects in cultured primary brain cells [12–15].

Subsequently, it was shown that PrP mutants lacking the TM1 domain or part of it are not converted into PrP^{Sc} [16]. Specifically, murine PrP mutants with deletions of residues 114–121 [17] or 112–119 [18] are not converted into PrP^{Sc}. Moreover, the deletion of 114–121 (henceforth termed PrPΔ114–121) led to a reduction in the level of PrP^{Sc} derived from endogenous PrP^C-wt in scrapie-infected Neuro2a cells, *i.e.* the deletion mutant had a dominant-negative effect on PrP^{Sc} accumulation [17].

Recently, we investigated in a collaborative study the effect of PrPΔ114–121 in transgenic mice with respect to the physiological function of PrP^C [19]. We could show that the PrPΔ114–121 mutant was not intrinsically toxic in the presence or absence of PrP^C. Co-expression of PrPΔ114–121 with other deletion mutants showed that it alleviates the pathogenic effect of the PrPΔ32–134 mutant, which is characterized by a spontaneous, non-infectious neurodegenerative syndrome distinct from prion disease. By contrast, PrPΔ114–121, enhanced the pathogenic effect of the PrPΔ94–134 deletion mutant. In another study published simultaneously the effect of PrPΔ105–125 in transgenic mice was investigated [20]. Both studies concluded that PrP^C acts neuroprotective via constitutive activation of a putative PrP receptor. Conversion of PrP^C into PrP^{Sc} might disrupt the interaction between PrP^C and the PrP receptor, although the detailed molecular mechanism is still unclear. Likewise, the mechanism underlying the inconvertibility of PrPΔ114–121 into PrP^{Sc} has not been resolved so far. A key to fully understand the function of the TM1 domain in PrP is the combination of data from different methodological approaches such as transgenic mice, cell biological model systems and biochemical structural studies. In this study we investigated the structural consequences of deleting residues 114–121 in murine PrP^C.

2. Materials and methods

2.1. Plasmid construction

For recombinant protein expression, the cDNA of murine PrP coding for amino acids 23–230 was cloned into the *E. coli* expression vector pRSET A (Invitrogen) yielding pRSET A::PrP-wt. The expression vector for PrPΔ114–121, pRSET A::PrPΔ114–121, was constructed by subcloning the fragment of PrPΔ114–121 obtained by digesting pUC19::PrPΔ114–121 [17] with *Eco*81I and *Eco*91I (MBI-Fermentas) into pRSET A::PrP-wt. The correct insertion was checked by DNA sequencing.

2.2. Recombinant protein expression and purification

PrP-wt and PrPΔ114–121 were expressed in *E. coli* BL21(DE3) as hexahistidine (His_6)-tagged fusion proteins and purified to homogeneity as published previously [21]. Briefly, inclusion bodies of the recombinant protein were denatured and subjected to affinity chromatography on nickel-NTA agarose. The protein was refolded and oxidized while immobilized on the column, followed by elution with buffer containing imidazole. The His_6-tag was then removed by thrombin cleavage. After ion-exchange chromatography, the protein was dialyzed against water and lyophilized. Purity was checked by SDS-PAGE.

2.3. Analytical methods

Protein concentrations of PrP-wt and PrPΔ114–121 were determined from the absorbance at 278 nm with the specific extinction coefficient $\varepsilon_{278\ nm}=63.130\ M^{-1}\ cm^{-1}$ calculated from the amino acid sequence (www.expasy.org/tools/protparam.html). The presence of the disulfide bond was checked using disodium 2-nitro-5-sulfonatosulfanyl-benzoate [22].

2.4. CD spectroscopy

Circular dichroism (CD) spectra were recorded at 298 K with a spectropolarimeter J-715 (Jasco) at protein concentrations of 20 to 75 μM in 0.10 cm and 0.01 cm quartz cells. The lyophilized protein was dissolved in 20 mM NEM

in D_2O, pD 7.0. At least four spectra were recorded between 260 and 180 nm, averaged and corrected for the buffer spectrum. The secondary structure content of PrP-wt and PrPΔ114–121 was calculated by a least-square fit according to Chang et al. [23] implemented into the interface Dicroprot [24], which uses a base set of four CD spectra typical for each type of secondary structure. Furthermore the secondary structure content was assessed with the programs SELCON [25], CONTINLL [26] and CDSSTR [27] using a base set of 43 CD spectra of proteins with known structure. The latter 3 programs are implemented in the interface CDPro [28].

The stability of the protein against denaturation was assessed using guanidine hydrochloride (GdnHCl) by adding aliquots of a 7 M GdnHCl stock solution (pH 6.0) to PrP-wt or PrPΔ114–121 (concentration: 15 μM, in 20 mM MES in D_2O, pD 6.0) and measuring the ellipticity at 222 nm. The values were recorded ten times and averaged. Assuming a two-state folding mechanism, the difference in free energy (ΔG) between folded and unfolded state is calculated according to Pace:

$$\Delta G = -RT \ln [Fd/(1 - Fd)]$$

where R is the gas constant, T the absolute temperature and Fd the fraction of unfolded protein [29]. The data from the denaturation experiments were analyzed by a nonlinear least-square fit using the program Origin version 7.0 (Origin Lab).

2.5. FTIR spectroscopy

All measurements were performed in D_2O, which does not adsorb in the region of the amide I transitions of the peptide backbone. Lyophilized PrP was dissolved in D_2O. The pD was adjusted to 7.2 by addition of concentrated DCl or NaOH. The samples were equilibrated overnight at room temperature in order to achieve complete proton–deuterium exchange of the backbone amides. The protein concentration was 150 μM throughout. Spectra were recorded at 293 K on a Bruker Tensor 27 FTIR spectrometer accumulating 128 scans at a resolution of 2 cm^{-1}; spectra of D_2O were recorded under the same conditions and subtracted from the sample spectra. The position of individual IR transitions in the amide I′ region between 1700 and 1600 cm^{-1} was resolved by second order derivative spectra. For protein secondary structure analysis the spectra were fitted with a set of 8 Lorentzian line shaped transitions.

2.6. EPR spectroscopy

Spectra were recorded on a Bruker Elexsys 500 instrument, with the following settings: microwave frequency 9.34 GHz (X-band), microwave power 0.2–4 mW, modulation frequency 100 kHz, modulation amplitude 1 mT, temperature 22 K; 10 spectra between 240 and 380 mT were averaged for each sample.

The protein was 20 μM in 25 mM NEM buffer+20% (v/v) glycerol in D_2O, pD 7.0. Copper(II) was added as $CuSO_4$. Only 0.9 equivalents of Cu^{2+} were added in order to selectively probe the Cu^{2+}-binding site close the TM1 region of PrP. The concentration of $CuSO_4$ stock solutions was determined by flame atomic absorption spectrometry (SpectrAA-110, Varian Inc.). The EPR samples (250 μl, 4-mm standard quartz tube) were frozen in an *iso*-pentane bath cooled with liquid nitrogen to 173 K and stored in liquid nitrogen prior to the measurement.

3. Results

3.1. Protein expression and purification

In order to characterize the consequences of deleting aa 114–121 for the structure of murine PrP, we expressed PrP-wt and PrPΔ114–121 in *E. coli* as recombinant proteins and purified them to homogeneity. The applied method for protein purification and refolding was shown to yield highly structurally homogenous protein preparations [21,30,31]. Both, PrP-wt and PrPΔ114–121, contained the structurally essential disulfide bond and displayed comparable solubility.

3.2. Structural analysis of PrP-wt and PrPΔ114–121 by FTIR and CD spectroscopy

For the structural analysis of PrP-wt and PrPΔ114–121 at pH 7.0, we applied FTIR spectroscopy to monitor amide I′ oscillations between 1700 and 1600 cm^{-1}. The amide I band represents predominantly C=O and C–N vibrations of the peptide backbone that are sensitive towards the hydrogen bonding pattern and thereby reflect the different types of secondary structure. In D_2O the proton of the amide group is exchanged with the deuterium ion, and consequently the positions of the bands shift to smaller wavenumber (amide I′ band). The FTIR spectra of PrP-wt and PrPΔ114–121 had a very similar shape (Fig. 2A, B) except for the region around 1615 cm^{-1} (Fig. 2C). The transition in this region is typical for antiparallel β-sheets, and already suggested a higher content of antiparallel β-sheets in PrPΔ114–121. For a detailed analysis of the secondary structure content of PrP-wt and PrPΔ114–121

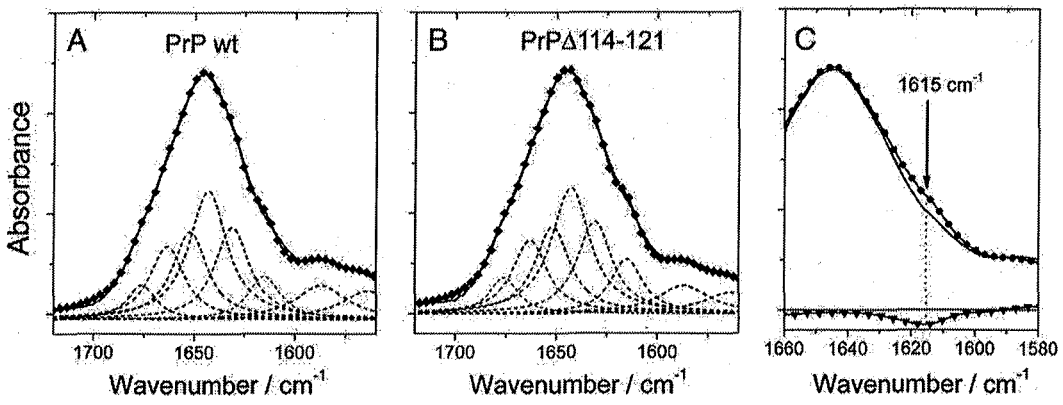

Fig. 2. Analysis of murine PrP-wt and PrPΔ114–121 by FTIR spectroscopy. (A) Component analysis of FTIR spectrum of PrP-wt and (B) of PrPΔ114–121. The amide I′ region is deconvoluted into 8 Lorentzian line shaped IR transitions (broken lines). In panels A and B the sum of the single components (lines with diamonds) overlay the experimental spectra (solid lines). (C) Overlay of FTIR spectra of PrP-wt and PrPΔ114–121. The solid line represents PrP-wt, the line with circles represents the spectrum of PrPΔ114–121. The difference spectrum (PrP-wt minus PrPΔ114–121) is shown as line with triangles and exhibits a minimum at 1615 cm^{-1}.

Table 1
Component analysis of FTIR spectra of PrP-wt and PrPΔ114–121

Secondary structure	Amide I′ wavenumber (cm^{-1})	PrP-wt	PrPΔ114–121
		Secondary structure content (%)	Secondary structure content (%)
Antiparallel β-sheet	1615	10.1	11.9
Parallel β-sheet	1629	15.0	16.2
β-turn	1664, 1675	17.1	18.0
random coil	1643	35.2	31.9
α-helix	1653	22.6	22.0

the spectra were fitted by a set of 8 Lorentzian line shaped IR transitions (Fig. 2B). Six out of 8 transitions could be assigned to contributions of α-helix (1652 cm^{-1}), β-sheet (1631 cm^{-1}), turns (~1664 cm^{-1} and ~1676 cm^{-1}), and random coil (1642 cm^{-1}) (Table 1). Two bands at 1587 and 1564 cm^{-1} were assigned to contributions of amino acid sidechains. Integration of the 6 bands revealed for both proteins a content of 22% α-helix, 25–28% β-sheet, 17–18% β-turns, and 32–35% random coil (Table 1). The analysis revealed clearly a structural difference between PrP-wt and PrPΔ114–121. PrPΔ114–121 displayed a higher content of antiparallel as well as parallel β-sheets and β-turns and correspondingly a lower random content than PrP-wt.

In order to estimate the consequences of deleting residues 114–121 might have for the structure of PrP, we performed secondary structure predictions for the PrP peptides aa 100–150 and the corresponding deletion mutant by nnPredict [32]. The prediction for the wt peptide is in reasonable agreement with the structure of mouse PrP 121–231 as determined by NMR [33]. The first β-sheet encompassing residues 128–131 is predicted by nnPredict and there is some propensity (Fig. 3) for an α-helix at the position of helix 1 (residues 144–153) of mouse PrP [33]. Furthermore, a long hydrophobic helix (108–119) is predicted in the TM1 region (residues 111–134). This helix is present in PrP when it is inserted in the membrane, whereas PrP in solution does not show any secondary structure of this region at pH 4.5 or pH 7.0 [34,35]. The prediction for the corresponding peptide (PrP 100–150, Δ114–121) suggests that the deletion eliminates the possibility of α-helix formation, but instead supports the formation of another short β-sheet at residues 108–110. This short β-sheet could align antiparallel to the existing β-sheets and give rise to the observed signal in FTIR.

In order to substantiate the changes in secondary structure observed by FTIR spectroscopy, we recorded CD spectra of PrP-wt and PrPΔ114–121 for secondary structure analysis (Fig. 4). CD spectra were recorded between 180 and 260 nm, which is a prerequisite for reliable estimates of the secondary structure content. Overlay of the CD spectra of PrP-wt and PrPΔ114–121 revealed that the latter exhibited more intense bands around 190 nm and 208 nm, but not at 222 nm (Fig. 4A). The constant intensity of the CD bands at 222 nm, where only α-helices contribute significantly, suggests that the content of α-helix did not change. The bands at 208 and 190 nm, on the other hand, contain spectral contributions from β-sheets, β-turns and random coil [27]. The calculated difference spectrum of PrPΔ114–121 minus PrP-wt resembles closely the spectrum of β-sheet structures computed from CD spectra of 15 different proteins [23] underlining that an additional β-sheet has formed (Fig. 4B). For a quantification of the secondary structure in PrP-wt and PrPΔ114–121, the spectra were analyzed according to Chang et al. [23] and with the programs SELCON [25], CONTINLL [26] and CDSSTR [27]. The analysis revealed again a higher β-sheet content in PrPΔ114–121, thus corroborating the results form FTIR spectroscopy. The results from FTIR and CD analysis are compared in Table 2.

Overall, the estimates of the secondary structure content by both spectroscopic techniques, FTIR and CD, are in good agreement. Noteworthy, both methods reveal that the deletion of residues 114–121 in PrP lead to an increase of 2–3% in β-sheet content, and a concomitant 1–3% decrease in random coil, whereas the α-helix content stays constant. The data demonstrate that a part of the unstructured N-terminal domain of PrP-wt has converted into β-sheet in PrPΔ114–121. The 2–3% higher content of β-sheet of secondary structure elements corresponds to four additional residues forming

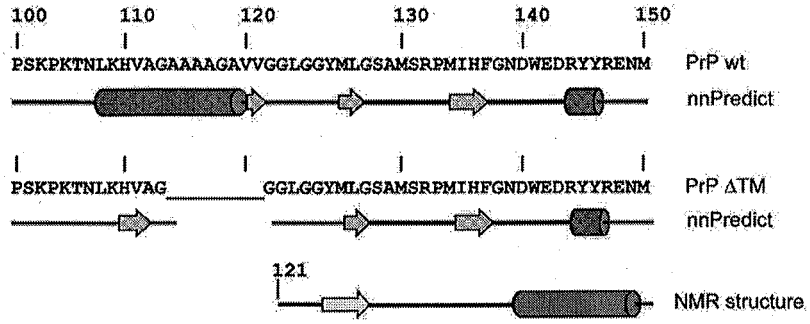

Fig. 3. Secondary structure prediction for PrP^C-wt and PrPΔ114–121 residues 100–150. The sequences of mouse PrP 100–150 and the corresponding sequence of PrPΔ114–121 are shown. Underneath, the secondary structure predictions by nnPredict [32] for both sequences is shown as shaded arrows (β-sheet) and red cylinders (α-helix). At the bottom is shown the secondary structure of mouse PrP^C as determined by NMR (Riek et al.[33]). The figure illustrates that nnPredict successfully predicted β-sheet 1 (128–131) as well as partially helix I of PrP. Furthermore the helix predicted for residues 108–119 does actually form when PrP^C occurs as integral membrane protein (Hegde et al. [10]) underlining the correct prediction by nnPredict. According to nnPredict the deletion of residues 114–121 induces the formation of a short β-sheet.

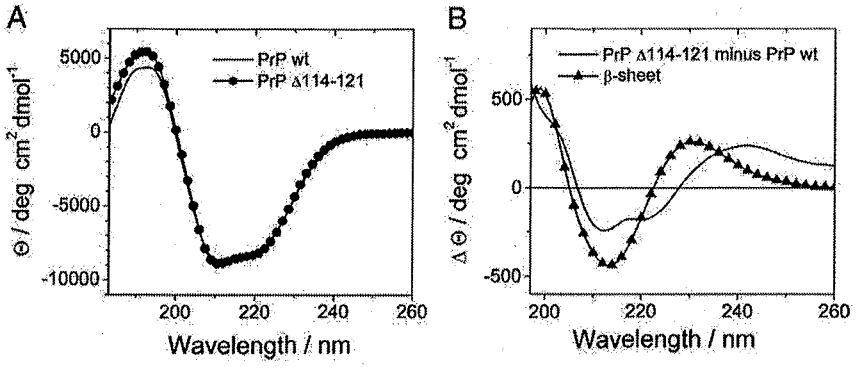

Fig. 4. (A) CD spectra of murine PrP-wt and PrPΔ114–121. The spectrum of PrP-wt is shown as a solid line (-) and the spectrum of PrPΔ114–121 as line with spheres (-●-). (B) CD difference spectrum of PrPΔ114–121 minus PrP-wt is shown as solid line (-) in comparison with the CD spectrum of a β-sheet structure computed from CD spectra of 15 different proteins (-▲-). The computed spectrum was adapted from Chang et al. [23] and divided by 10 to overlay with the difference spectrum.

main-chain hydrogen bonds. In a β-sheet, this would account for an excess of ~2 hydrogen bonds in PrPΔ114–121compared to PrP-wt, which should stabilize protein. In order to test if PrPΔ114–121 possesses higher conformational stability than PrP-wt, we performed chemical denaturation experiments.

3.3. Analysis of protein stability by chemical denaturation

PrP-wt and PrPΔ114–121 were unfolded by increasing concentrations of the denaturing agent GdnHCl, and the ellipticity at 222 nm was recorded. The unfolding/folding of the C-terminal structured domain of PrP is fully reversible under these conditions [36]. The denaturation curves for both proteins are shown in Fig. 5. Analysis of the data by a least-square fit [29] yielded the difference in free energy ΔG^0 between folded and unfolded state. For PrP-wt a ΔG^0 of 21.4±0.3 kJ mol^{-1} was determined. A significantly higher stability with ΔG^0 equaling to 24.8±0.4 kJ mol^{-1} was found for PrPΔ114–121. The $\Delta\Delta G^0$ of 3.4±0.3 kJ mol^{-1} would account for 1–2 additional hydrogen bonds in PrPΔ114–121. Thus, the deletion of the amino acids 114–121 in PrP results in a stabilization of the overall protein structure.

3.4. EPR spectroscopic analysis of copper(II) binding to PrP-wt and PrP ΔTM

The deleted residues 114–121 in PrP are located very closely to a Cu^{2+} binding site that is remote from the octarepeat structure [9,37]. This site coordinates Cu^{2+} through the imidazole nitrogen of His111 (His110 in mouse PrP) and most likely through backbone nitrogen or one methionine sulphur [38–40]. In competition experiments it was shown that peptides encompassing the TM1 domain (aa 91–115) bind Cu^{2+} with higher affinity than the octarepeats (aa 58–91) [9]. Cu^{2+} binding to this site induces β-sheet formation [9] and conversion of PrP^C into a protease-resistant species [41]. The peptide PrP 106–126 which harbors this Cu^{2+}-binding site, is cytotoxic [14,42,43] to PrP^C-expressing cells, and this sequence is essential for the conversion of PrP^C into PrP^{Sc} [44]. Interestingly, Cu^{2+} binding to this peptide promotes aggregation and the formation of fibrils [45].

We examined the effects of deleting residues 114–121 on the binding of Cu^{2+} to PrP^C by EPR spectroscopy. Only 0.9 equivalents of Cu^{2+} per PrP-wt or PrPΔ114–121 were added. As this site displays higher affinity to Cu^{2+} than do the octarepeats, the added Cu^{2+} binds predominantly there [9].

EPR spectra of Cu^{2+}-bound PrP-wt and Cu^{2+}-bound PrPΔ114–121 were typical of type II Cu in a square planar geometry [46]. Both Cu–protein complexes exhibited the same g and A parameters, $g_\parallel$=2.26, $A_\parallel$=17 mT and in the $g^\perp$ region a crossover at g=2.06. There were some differences in the $g^\perp$ region (Fig. 6A, B) which indicate the presence of a small amount of a radical in the PrP-wt sample. The EPR parameters $g_\parallel$ and $A_\parallel$ are sensitive to the geometry and nature of the bound ligands. Comparison of the parameters obtained here with those from several model compounds suggests that Cu^{2+} is coordinated by a set of N/O ligands [46]. The $g^\perp$ region was

Table 2
Secondary structure content of PrP-wt and PrPΔ114–121

PrP	Wt					Δ114–121				
Method	FTIR	CD				FTIR	CD			
		CONTINLL	SELCON	CDSSTR	Chang		CONTINLL	SELCON	CDSSTR	Change
α-helix (%)	22.6	20.0	19.2	18.6	20.4	22.0	20.1	19.1	18.6	20.7
β-sheet (%)	25.1	24.9	26.5	25.6	21.6	28.1	26.2	28.4	26.9	24.1
β-turn (%)	17.1	21.7	22.0	22.4	22.7	18.0	21.1	21.1	22.6	20.7
Random coil (%)	35.2	33.4	33.4	33.3	35.6	31.9	32.6	30.9	32.6	34.5

Comparison of CD and FTIR data.

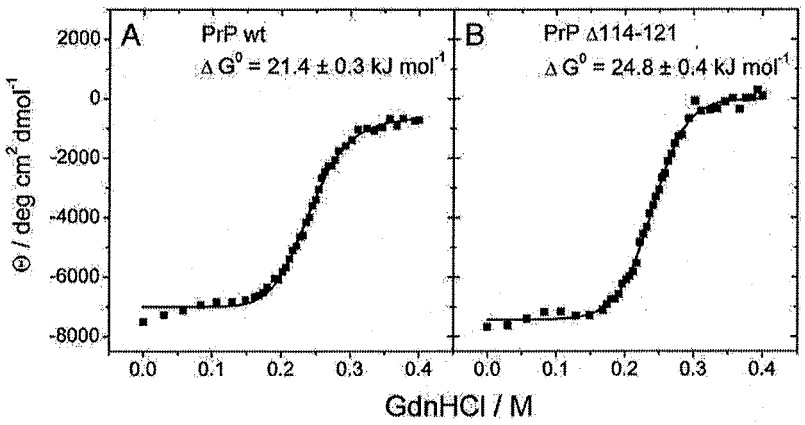

Fig. 5. Stability of murine PrP-wt and PrPΔ114–121 assessed by chemical denaturation with GdnHCl. Denaturation curves of PrP-wt (A) and PrPΔ114–121 (B) are shown.

further analyzed by taking the derivative of the recorded spectra to resolve for additional splittings from coordinated nitrogens (I=1 for ^{14}N). At least seven equidistant lines could be resolved

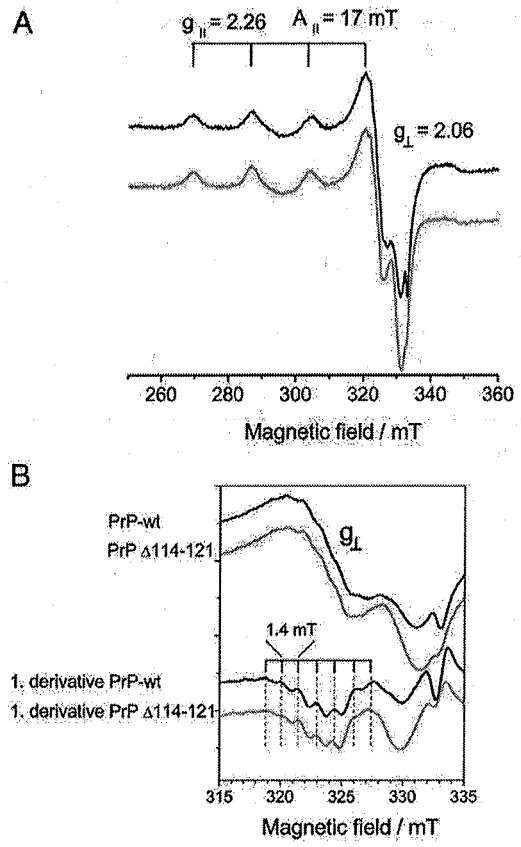

Fig. 6. Cu^{2+} binding to PrP-wt and PrPΔ114–121 monitored by EPR spectroscopy. Protein 20 μM in 25 mM NEM buffer+20% (v/v) glycerol in D_2O, pD 7.0. Instrument settings: microwave frequency, 9.342 GHz; microwave power, 2 mW; modulation amplitude, 1 mT, temperature, 22 K. (A) Upper black trace, PrP-wt; red trace, PrPΔ114–121. (B) $g^{\perp}$ region of Cu^{2+}-PrP-wt and Cu^{2+}-PrPΔ114–121. The lower traces represent the first derivative of the recorded spectra to document the presence of additional splittings due to nitrogen couplings.

(splitting ≈ 1.4 mT; Fig. 6B) which were attributed to nitrogen superhyperfine coupling of 3–4 nitrogen atoms bound to Cu^{2+}. This is in agreement with a recent study on Cu^{2+}-binding to the PrP 90–126 peptide [47] and further supported by a EXAFS study which suggests that Cu^{2+} is coordinated by one S and three N atoms to the PrP 106–114 peptide [39,40]. In summary, the Cu^{2+} binding to the PrP protein was marginally affected, if at all, by the deletion of residues 114–121.

4. Discussion

In this study, we investigated the influence of the deleting residues 114–121 of mouse PrP on protein structure, stability and Cu^{2+} binding properties. Previous work in scrapie-infected cell cultures had shown that this deletion mutant is resistant to conversion into PrP^{Sc} [17]. FTIR spectroscopic analysis in this study revealed a higher content of β-sheet structure in the mutant protein. The CD spectra obtained in the present study are very similar to those of mouse PrP 23–231 or human PrP 23–231 in previous studies [21,34] and the CD intensity at 222 nm of −8.000 to −9.000 deg $dmol^{-1}$ cm^2 demonstrate a content of 20–22% α-helix in PrP-wt (23–231). Thus, the proteins prepared in the different studies have the same secondary structure content. By contrast, the secondary structure content of mouse PrP as derived from the NMR structure of mouse PrP 121–231 [33] and assuming that the N-terminal region 23–121 is not folded yields about 27.7% α-helical content. Clearly, the secondary structure content calculated by CD and FTIR spectroscopy deviates from the structure determined by NMR spectroscopy. The difference is more pronounced comparing the β-sheet content of PrP^C calculated by CD and FTIR spectroscopy with the structural data. Again, assuming that the N-terminal part of PrP-wt (23–121) contains no β-sheet, one calculates the β-sheet content from the NMR structural data to 2%, whereas the CD and FTIR spectroscopic data strongly support a β-sheet content of 25–28%. The content of β-turns in the structures of mouse PrP^C 23–231 was judged from the structural information on mouse PrP^C 121–231 and from the structural data of three octarepeats (human PrP 61–84) determined by NMR [48] using the program STRIDE [49].

Assuming that the other regions of the N-terminal domain 23–121 adopt a random coil conformation one calculates the β-turn content to 22%. This value is in fair agreement with the values obtained from FTIR and CD spectroscopy (17–21%, Table 2). The largest uncertainty in the calculation of the secondary structure content arises from the lack of structural data for the N-terminal region. Two NMR studies have shown that this region does not adopt a complete random coil conformation. Especially the octarepeat regions form β-turns [48], and further regions in the N-terminus encompassing at least 10 more residues exist in mixed populations of random coil and a structured state [50]. However, the apparent deviation in secondary structure content determined by NMR and calculated from CD and FTIR spectra is most likely due to incorrect assignments of β-turn and β-sheet transition bands in FTIR as well as in CD spectroscopy. We performed our fits and assignments of FTIR bands in agreement with recent FTIR studies on PrP [51–53] or general studies on protein secondary structure analysis [54]. However, there is also a detailed spectroscopic study on β-turns, where the authors assign a band around 1640 cm^{-1} of the amide I region (*i.e.* ~1635 cm^{-1} in D_2O) to β-turn instead to β-sheets [55]. The situation is similar in CD spectroscopy. A study showed that the β-turns type I and type II contribute differently to the CD spectrum and can largely overlay the bands of β-sheet structures [56]. Therefore the quantification of all secondary structure components by FTIR and CD spectroscopy remains difficult. Nevertheless, the comparison of the spectra of PrP^C-wt and PrPΔ114–121 yields valuable information on structural changes in the deletion mutant. We identified an increase of a band centered at 1615 cm^{-1} in the amide I′ region of PrPΔ114–121 (Fig. 3). The assignment of this band to antiparallel β-sheets is well established and is evidence for an additional short β-sheet in PrPΔ114–121. In general, antiparallel β-sheets are more reliably estimated from FTIR spectra than from CD spectra [54]. The analysis of the CD spectra of PrP-wt and PrPΔ114–121 (Fig. 4B) supports this observation (Table 2). The formation of a short β-sheet encompassing residues 110–112 in PrPΔ114–121 is also suggested by nnPredict (Fig. 3). It is in proximity to β-sheet 1 and might arrange antiparallel to this structure, thus stabilizing this region as confirmed by unfolding experiments using chemical denaturation (Fig. 5). The folding energy of PrP-wt 23–231 of -21.4 ± 0.3 kJ mol^{-1} was very similar to the value determined by Hornemann and Glockshuber [36] for PrP 121–231 with $\Delta G^0=-21.8\pm1.4$ kJ mol^{-1} at pH 7.0 in 20 mM sodium phosphate buffer, suggesting that the N-terminal region does not significantly contribute to the overall stability of the protein. The increased stability of PrPΔ114–121 with a folding energy of -24.8 ± 0.4 kJ mol^{-1} accounts for approximately 1 or 2 additional hydrogen bonds, as expected by the formation of a short strand of antiparallel β-sheet.

The small changes in the overall structure of PrPΔ114–121 compared to PrP-wt argue for an at least partial preservation of PrP's physiological function. This is supported by our recent observation that expression of PrPΔ114–121 in mice on a $Prp^{-/-}$ background, which did not cause any pathogenic effect by itself, diminished the pathogenic effect of the deletion mutant PrPΔ32–134 in transgenic mice [19] although the rescue effect was weaker than that of PrP-wt [57,58]. In stark contrast, co-expression of PrPΔ114–121 aggravated the pathogenic effect of another deletion mutant, PrPΔ94–134 (termed PrPΔCD), that is rescued by PrP-wt [19], which is clear evidence for a fundamental difference between PrPΔ114–121 and PrP-wt at the functional level. Interestingly, our recent topology studies revealed that deletion of residues 114–121 leads to the complete loss of the transmembrane topology and of α-cleavage of PrP^C [59].

The structural changes in PrPΔ114–121 discovered in the present work point to two possible mechanisms of how the deletion of residues 114–121 might abolish the conversion into PrP^{Sc}. The first possibility is that the region around the deletion is required for transient destabilization followed by structural conversion of PrP^C into PrP^{Sc} as indicated by several studies [17,18,44,60]. The minimal infectious unit is represented by PrP^{Sc} that is based on the conversion of "PrP^C106", representing a molecule with deletion of both, residues 23–88 and 141–176, yet comprising the region 90–121 [16]. It was shown that the region around residues 109–120 undergoes a major conformational change in PrP^{Sc}, since antibodies directed against this region recognize PrP^C but not PrP^{Sc} [61]. Therefore some structural change in the TM1 region seems to be required for the transition of PrP^C into PrP^{Sc}. Our results suggest that in PrPΔ114–121 this region is stabilized by an additional β-sheet, which might represent an additional energetic barrier blocking the pathway of PrP^C to PrP^{Sc} conversion. Although a study by Liemann and Glockshuber [62] has shown that destabilization of PrP^C is not a general mechanism underlying the formation of PrP^{Sc}, the reverse conclusion that stabilization of PrP^C blocks conversion to PrP^{Sc} still can hold true. Indeed a study by Baskakov et al. [63] strongly supports this hypothesis. Baskakov et al. demonstrated that there is an energetic barrier between the α-helical state and the energetically favored β-sheet rich state. The α-helical PrP^C is kinetically trapped in a local minimum separated by a large energetic barrier from the β-sheet rich state, which is most likely similar to PrP^{Sc}. Thus, the increase of the energetic barrier by a stabilization of PrPΔ114–121 forms a deeper trap for the α-helical PrP^C and blocks conversion into PrP^{Sc}.

The second possibility of how the conversion of PrPΔ114–121 into PrP^{Sc} might be blocked is the loss of the binding site between PrP^C and PrP^{Sc}. Association between PrP^C and PrP^{Sc} is required for the conversion of PrP^C and PrP^{Sc} accumulation. Norstrom and Mastrianni [18] presented evidence that the palindromic sequence AGAAAAGA (residues 112–119) is necessary for the binding of PrP^C to PrP^{Sc}. One cannot exclude that the binding occurs also via neighboring residues close to the palindromic sequence. We observed that the deletion of residues 114–121 led to the formation of a short β-sheet most likely close to this site. Deletion of residues 112–119 may well result in a similar structural change. Such a conformational change might cover the recognition site between PrP^C and PrP^{Sc} and therefore block the conversion of PrPΔ114–121 into PrP^{Sc}.

However, the second possibility describing the loss of the binding site in PrPΔ114–121 cannot explain the observed

phenotype of a dominant-negative effect on prion propagation [17]. The first model presented above including an additional β-sheet that energetically blocks the conversion of PrPΔ114–121 into PrP^{Sc} can indeed provide an explanation for the observed dominant-negative effect. The overall similar structure between PrPΔ114–121 and PrP^{C}-wt still enables the binding of the mutant to PrP^{Sc}. The deletion, however, renders the molecule inert with respect to the conversion process. This will break the chain of PrP^{Sc} accumulation and should ultimately prevent disease progression. Future prion inoculation studies of the transgenic mice carrying the PrPΔ114–121 gene [19] will be instrumental to verify *in vivo* the model proposed here.

Acknowledgements

We gratefully acknowledge the funding by the Deutsche Forschungsgemeinschaft through the "TransRegio-SFB 11 Konstanz-Zürich, Structure and function of membrane proteins", as well as by the EU Commission through the FP6 Network of Excellence "NeuroPrion"/subproject PrioGen.

References

[1] S.B. Prusiner, Prions, Proc. Natl. Acad. Sci. U. S. A. 95 (1998) 13363–13383.
[2] S.B. Prusiner, M. Scott, D. Foster, K.M. Pan, D. Groth, C. Mirenda, M. Torchia, S.L. Yang, D. Serban, G.A. Carlson, et al., Transgenetic studies implicate interactions between homologous PrP isoforms in scrapie prion replication, Cell 63 (1990) 673–686.
[3] R. Chiesa, D.A. Harris, Prion diseases: what is the neurotoxic molecule? Neurobiol. Dis. 8 (2001) 743–763.
[4] S. Brandner, A. Raeber, A. Sailer, T. Blättler, M. Fischer, C. Weissmann, A. Aguzzi, Normal host prion protein (PrP^{C}) is required for scrapie spread within the central nervous system, Proc. Natl. Acad. Sci. U. S. A. 93 (1996) 13148–13151.
[5] G. Mallucci, A. Dickinson, J. Linehan, P.C. Klohn, S. Brandner, J. Collinge, Depleting neuronal PrP in prion infection prevents disease and reverses spongiosis, Science 302 (2003) 871–874.
[6] H. Büeler, A. Aguzzi, A. Sailer, R.A. Greiner, P. Autenried, M. Aguet, C. Weissmann, Mice devoid of PrP are resistant to scrapie, Cell 73 (1993) 1339–1347.
[7] C.J. Choi, A. Kanthasamy, V. Anantharam, A.G. Kanthasamy, Interaction of metals with prion protein: possible role of divalent cations in the pathogenesis of prion diseases, Neurotoxicology 27 (2006) 777–787.
[8] G.L. Millhauser, Copper binding in the prion protein, Acc. Chem. Res. 37 (2004) 79–85.
[9] C.E. Jones, S.R. Abdelraheim, D.R. Brown, J.H. Viles, Preferential Cu^{2+} coordination by His96 and His111 induces β-sheet formation in the unstructured amyloidogenic region of the prion protein, J. Biol. Chem. 279 (2004) 32018–32027.
[10] R.S. Hegde, J.A. Mastrianni, M.R. Scott, K.A. DeFea, P. Tremblay, M. Torchia, S.J. DeArmond, S.B. Prusiner, V.R. Lingappa, A transmembrane form of the prion protein in neurodegenerative disease, Science 279 (1998) 827–834.
[11] R.S. Hegde, P. Tremblay, D. Groth, S.J. DeArmond, S.B. Prusiner, V.R. Lingappa, Transmissible and genetic prion diseases share a common pathway of neurodegeneration, Nature 402 (1999) 822–826.
[12] G. Forloni, N. Angeretti, R. Chiesa, E. Monzani, M. Salmona, O. Bugiani, F. Tagliavini, Neurotoxicity of a prion protein fragment, Nature 362 (1993) 543–546.
[13] L. De Gioia, C. Selvaggini, E. Ghibaudi, L. Diomede, O. Bugiani, G. Forloni, F. Tagliavini, M. Salmona, Conformational polymorphism of the amyloidogenic and neurotoxic peptide homologous to residues 106–126 of the prion protein, J. Biol. Chem. 269 (1994) 7859–7862.
[14] J. Ciesielski-Treska, N.J. Grant, G. Ulrich, M. Corrotte, Y. Bailly, A.M. Haeberle, S. Chasserot-Golaz, M.F. Bader, Fibrillar prion peptide (106–126) and scrapie prion protein hamper phagocytosis in microglia, Glia 46 (2004) 101–115.
[15] M. Ettaiche, R. Pichot, J.P. Vincent, J. Chabry, *In vivo* cytotoxicity of the prion protein fragment 106–126, J. Biol. Chem. 275 (2000) 36487–36490.
[16] T. Muramoto, M. Scott, F.E. Cohen, S.B. Prusiner, Recombinant scrapie-like prion protein of 106 amino acids is soluble, Proc. Natl. Acad. Sci. U. S. A. 93 (1996) 15457–15462.
[17] C. Hölscher, H. Delius, A. Bürkle, Overexpression of nonconvertible PrP^{C} delta114–121 in scrapie-infected mouse neuroblastoma cells leads to *trans*-dominant inhibition of wild-type PrP^{Sc} accumulation, J. Virol. 72 (1998) 1153–1159.
[18] E.M. Norstrom, J.A. Mastrianni, The AGAAAAGA palindrome in PrP is required to generate a productive PrP^{Sc}–PrP^{C} complex that leads to prion propagation, J. Biol. Chem. 280 (2005) 27236–27243.
[19] F. Baumann, M. Tolnay, C. Brabeck, J. Pahnke, U. Kloz, H.H. Niemann, M. Heikenwalder, T. Rülicke, A. Bürkle, A. Aguzzi, Lethal recessive myelin toxicity of prion protein lacking its central domain, Embo J. 26 (2007) 538–547.
[20] A. Li, H.M. Christensen, L.R. Stewart, K.A. Roth, R. Chiesa, D.A. Harris, Neonatal lethality in transgenic mice expressing prion protein with a deletion of residues 105–125, Embo J. 26 (2007) 548–558.
[21] R. Zahn, C. von Schroetter, K. Wüthrich, Human prion proteins expressed in *Escherichia coli* and purified by high-affinity column refolding, FEBS Lett. 417 (1997) 400–404.
[22] T.W. Thannhauser, Y. Konishi, H.A. Scheraga, Sensitive quantitative analysis of disulfide bonds in polypeptides and proteins, Anal. Biochem. 138 (1984) 181–188.
[23] C.T. Chang, C.S. Wu, J.T. Yang, Circular dichroic analysis of protein conformation: inclusion of the beta-turns, Anal. Biochem. 91 (1978) 13–31.
[24] G. Deleage, C. Geourjon, An interactive graphic program for calculating the secondary structure content of proteins from circular dichroism spectrum, Comput. Appl. Biosci. 2 (1993) 197–199.
[25] N. Sreerama, R.W. Woody, A self-consistent method for the analysis of protein secondary structure from circular dichroism, Anal. Biochem. 209 (1993) 32–44.
[26] S.W. Provencher, J. Glöckner, Estimation of globular protein secondary structure from circular dichroism, Biochemistry 20 (1981) 33–37.
[27] W.C. Johnson, Analyzing protein circular dichroism spectra for accurate secondary structures, Proteins 35 (1999) 307–312.
[28] N. Sreerama, R.W. Woody, Estimation of protein secondary structure from circular dichroism spectra: comparison of CONTIN, SELCON, and CDSSTR methods with an expanded reference set, Anal. Biochem. 287 (2000) 252–260.
[29] C.N. Pace, Conformational stability of globular proteins, Trends Biochem. Sci. 15 (1990) 14–17.
[30] R. Zahn, A. Liu, T. Luhrs, R. Riek, C. von Schroetter, F. Lopez Garcia, M. Billeter, L. Calzolai, G. Wider, K. Wüthrich, NMR solution structure of the human prion protein, Proc. Natl. Acad. Sci. U. S. A. 97 (2000) 145–150.
[31] R. Zahn, P. Güntert, C. von Schroetter, K. Wüthrich, NMR structure of a variant human prion protein with two disulfide bridges, J. Mol. Biol. 326 (2003) 225–234.
[32] D.G. Kneller, F.E. Cohen, R. Langridge, Improvements in protein secondary structure prediction by an enhanced neural network, J. Mol. Biol. 214 (1990) 171–182.
[33] R. Riek, S. Hornemann, G. Wider, M. Billeter, R. Glockshuber, K. Wüthrich, NMR structure of the mouse prion protein domain PrP(121–321), Nature 382 (1996) 180–182.
[34] S. Hornemann, C. Korth, B. Oesch, R. Riek, G. Wider, K. Wüthrich, R. Glockshuber, Recombinant full-length murine prion protein, mPrP(23–231): purification and spectroscopic characterization, FEBS Lett. 413 (1997) 277–281.
[35] L. Calzolai, R. Zahn, Influence of pH on NMR structure and stability of the

human prion protein globular domain, J. Biol. Chem. 278 (2003) 35592–35596.
[36] S. Hornemann, R. Glockshuber, Autonomous and reversible folding of a soluble amino-terminally truncated segment of the mouse prion protein, J. Mol. Biol. 261 (1996) 614–619.
[37] C.S. Burns, E. Aronoff-Spencer, G. Legname, S.B. Prusiner, W.E. Antholine, G.J. Gerfen, J. Peisach, G.L. Millhauser, Copper coordination in the full-length, recombinant prion protein, Biochemistry 42 (2003) 6794–6803.
[38] C.E. Jones, M. Klewpatinond, S.R. Abdelraheim, D.R. Brown, J.H. Viles, Probing copper^{2+} binding to the prion protein using diamagnetic nickel^{2+} and ^{1}H NMR: the unstructured N terminus facilitates the coordination of six copper^{2+} ions at physiological concentrations, J. Mol. Biol. 346 (2005) 1393–1407.
[39] E. Gaggelli, F. Bernardi, E. Molteni, R. Pogni, D. Valensin, G. Valensin, M. Remelli, M. Luczkowski, H. Kozlowski, Interaction of the human prion PrP(106–126) sequence with copper(II), manganese(II), and zinc(II): NMR and EPR studies, J. Am. Chem. Soc. 127 (2005) 996–1006.
[40] J. Shearer, P. Soh, The copper(II) adduct of the unstructured region of the amyloidogenic fragment derived from the human prion protein is redox-active at physiological pH, Inorg. Chem. 46 (2007) 710–719.
[41] E. Quaglio, R. Chiesa, D.A. Harris, Copper converts the cellular prion protein into a protease-resistant species that is distinct from the scrapie isoform, J. Biol. Chem. 276 (2001) 11432–11438.
[42] M.A. Deli, S. Sakaguchi, R. Nakaoke, C.S. Abraham, H. Takahata, J. Kopacek, K. Shigematsu, S. Katamine, M. Niwa, PrP fragment 106–126 is toxic to cerebral endothelial cells expressing PrP^{C}, Neuroreport 11 (2000) 3931–3936.
[43] S. Supattapone, P. Bosque, T. Muramoto, H. Wille, C. Aagaard, D. Peretz, H.O. Nguyen, C. Heinrich, M. Torchia, J. Safar, F.E. Cohen, S.J. DeArmond, S.B. Prusiner, M. Scott, Prion protein of 106 residues creates an artificial transmission barrier for prion replication in transgenic mice, Cell 96 (1999) 869–878.
[44] M. Fischer, T. Rülicke, A. Raeber, A. Sailer, M. Moser, B. Oesch, S. Brandner, A. Aguzzi, C. Weissmann, Prion protein (PrP) with amino-proximal deletions restoring susceptibility of PrP knockout mice to scrapie, Embo J. 15 (1996) 1255–1264.
[45] M.F. Jobling, X. Huang, L.R. Stewart, K.J. Barnham, C. Curtain, I. Volitakis, M. Perugini, A.R. White, R.A. Cherny, C.L. Masters, C.J. Barrow, S.J. Collins, A.I. Bush, R. Cappai, Copper and zinc binding modulates the aggregation and neurotoxic properties of the prion peptide PrP106–126, Biochemistry 40 (2001) 8073–8084.
[46] J. Peisach, W.E. Blumberg, Structural implications derived from the analysis of electron paramagnetic resonance spectra of natural and artificial copper proteins, Arch. Biochem. Biophys. 165 (1974) 691–708.
[47] M. Klewpatinond, J.H. Viles, Fragment length influences affinity for Copper^{2+} and Nickel^{2+} binding to His96 or His111 of the prion protein and spectroscopic evidence for a multiple His binding only at low pH, Biochem. J. 404 (2007) 393–402.
[48] R. Zahn, The octapeptide repeats in mammalian prion protein constitute a pH-dependent folding and aggregation site, J. Mol. Biol. 334 (2003) 477–488.
[49] D. Frishman, P. Argos, Knowledge-based protein secondary structure assignment, Proteins 23 (1995) 566–579.
[50] N. Kachel, W. Kremer, R. Zahn, H.R. Kalbitzer, Observation of intermediate states of the human prion protein by high pressure NMR spectroscopy, BMC Struct. Biol. 6 (2006) 16.
[51] J. Watzlawik, L. Skora, D. Frense, C. Griesinger, M. Zweckstetter, W.J. Schulz-Schaeffer, M.L. Kramer, Prion protein helix1 promotes aggregation but is not converted into β-sheet, J. Biol. Chem. 281 (2006) 30242–30250.
[52] O.V. Bocharova, L. Breydo, A.S. Parfenov, V.V. Salnikov, I.V. Baskakov, In vitro conversion of full-length mammalian prion protein produces amyloid form with physical properties of PrP(Sc), J. Mol. Biol. 346 (2005) 645–659.
[53] Y. Cordeiro, J. Kraineva, R. Ravindra, L.M. Lima, M.P. Gomes, D. Foguel, R. Winter, J.L. Silva, Hydration and packing effects on prion folding and β-sheet conversion. High pressure spectroscopy and pressure perturbation calorimetry studies, J. Biol. Chem. 279 (2004) 32354–32359.
[54] R. Pribic, I.H. van Stokkum, D. Chapman, P.I. Haris, M. Bloemendal, Protein secondary structure from Fourier transform infrared and/or circular dichroism spectra, Anal. Biochem. 214 (1993) 366–378.
[55] M. Hollosi, Z. Majer, A.Z. Ronai, A. Magyar, K. Medzihradszky, S. Holly, A. Perczel, G.D. Fasman, CD and Fourier transform IR spectroscopic studies of peptides. II. Detection of β-turns in linear peptides, Biopolymers 34 (1994) 177–185.
[56] A. Perczel, G.D. Fasman, Quantitative analysis of cyclic β-turn models, Protein Sci. 1 (1992) 378–395.
[57] D. Shmerling, I. Hegyi, M. Fischer, T. Blättler, S. Brandner, J. Götz, T. Rülicke, E. Flechsig, A. Cozzio, C. von Mering, C. Hangartner, A. Aguzzi, C. Weissmann, Expression of amino-terminally truncated PrP in the mouse leading to ataxia and specific cerebellar lesions, Cell 93 (1998) 203–214.
[58] I. Radovanovic, N. Braun, O.T. Giger, K. Mertz, G. Miele, M. Prinz, B. Navarro, A. Aguzzi, Truncated prion protein and Doppel are myelinotoxic in the absence of oligodendrocytic PrP^{C}, J. Neurosci. 25 (2005) 4879–4888.
[59] J. Lutz, C. Brabeck, H.H. Niemann, C. Korth, J. Collinge, V.R. Lingappa, A. Bürkle, Microdeletions within the hydrophobic core region alter topology and metabolism of cellular prion protein (unpublished data).
[60] V.A. Lawson, S.A. Priola, K. Wehrly, B. Chesebro, N-terminal truncation of prion protein affects both formation and conformation of abnormal protease-resistant prion protein generated in vitro, J. Biol. Chem. 276 (2001) 35265–35271.
[61] D. Peretz, R.A. Williamson, Y. Matsunaga, H. Serban, C. Pinilla, R.B. Bastidas, R. Rozenshteyn, T.L. James, R.A. Houghten, F.E. Cohen, S.B. Prusiner, D.R. Burton, A conformational transition at the N-terminus of the prion protein features in formation of the scrapie isoform, J. Mol. Biol. 273 (1997) 614–622.
[62] S. Liemann, R. Glockshuber, Influence of amino acid substitutions related to inherited human prion diseases on the thermodynamic stability of the cellular prion protein, Biochemistry 38 (1999) 3258–3267.
[63] I.V. Baskakov, G. Legname, S.B. Prusiner, F.E. Cohen, Folding of prion protein to its native alpha-helical conformation is under kinetic control, J. Biol. Chem. 276 (2001) 19687–19690.